

A near-ideal dechirper for plasma-based electron and positron acceleration using a hollow channel plasma

Y. P. Wu,¹ J. F. Hua,^{1,*} C. H. Pai,¹ W. An,² X. L. Xu,² C. J. Zhang,² F. Li,² Y. Wan,¹ Z. Nie,¹ Z. Zhou,¹ J. Zhang,¹ S. Liu,¹ S. Y. Zhou,¹ B. Peng,¹ Y. Fang,¹ W. Lu,^{1,†} W. B. Mori,² and C. Joshi²

¹*Department of Engineering Physics, Tsinghua University, Beijing 100084, China*

²*University of Los Angeles, Los Angeles, California 90095, USA*

(Dated: July 21, 2022)

Plasma-based electron and positron wakefield acceleration has made great strides in the past decade. However one major challenge for its applications to coherent light sources and colliders is the relatively large energy spread of the accelerated beams, currently at a few percent level. This energy spread is usually correlated with particle position in the beam arising from the longitudinal chirp of the wakefield amplitude. Therefore a dechirper is highly desirable for reducing this spread down to $\sim 0.1\%$ level, while at the same time for maintaining the emittance of the accelerated beam. Here we propose that a low-density hollow channel plasma can act as a near-ideal dechirper for both electrons and positrons. We demonstrate the concept through large-scale three-dimensional particle-in-cell simulations. We show that the initial positive correlated energy spread (chirp) on the beam exiting a plasma accelerator can be compensated by the nearly linear self-wake induced by the beam in the hollow channel from few percent level down to $\leq 0.1\%$. Meanwhile, the beam emittance can be preserved due to the negligible transverse field inside the channel. This passive method may significantly improve the beam quality of plasma-based accelerators, paving the way for their applications to future compact free electron lasers and colliders.

A plasma wake driven by an intense laser pulse or a charged particle beam can be utilized to accelerate electrons and positrons at extremely large accelerating fields of ≥ 100 GV/m, which are orders of magnitude larger than those in state-of-the-art radio-frequency microwave based accelerators [1, 2]. In the past decade, plasma-based wakefield acceleration has achieved many significant milestones, such as multi-GeV electron acceleration in laser driven wakes [3–10], and high-energy, high-efficiency electron/positron acceleration in beam driven wakes [11–14]. However, for the beams produced by plasma accelerators to be useable for critical applications like X-ray free electron lasers (X-FELs) and linear colliders, many challenges still remain. One of these is the relatively large energy spread of the accelerated electron/positron beams produced by plasma

accelerators. Currently the experimentally achieved energy spread is typically a few percent, which is about one to two order of magnitude larger than that is required for X-FELs and colliders operating at the energy frontier of particle physics.

Before one can invent ways to reduce the energy spread, it is imperative to understand why the energy spread comes about. In order to obtain high gradients, the plasma accelerator must be operated in a high-density plasma which in turn means that the wavelength of the accelerating structure is microscopic (tens to hundreds of micrometers). Due to the very short wavelength of this structure, the acceleration phase interval occupied by the short electron/positron beams is much larger than that in a traditional accelerator. This can lead to a significant energy chirp in the beam unless ideal beam loading can be achieved [15, 16]. This chirp is typically much larger than the intrinsic slice energy spread of the beam. For example, in many recently proposed injection schemes, the intrinsic energy spread of the beam slices could be reduced down to ~ 1 MeV or even tens of keV level [17–21], therefore, for beam energies more than a few hundred MeV, the energy chirp induced by the acceleration phase variance becomes the dominant part of the total energy spread.

In principle, direct reduction of this energy chirp down to $\sim 0.1\%$ level in a single-stage plasma accelerator is possible through subtle parameter fine-tuning. However, such fine-tuning may prove to be extremely challenging in practice. Here we propose a two-step strategy that may be more realistic and robust. In the first step, a stable positively-chirped beam (the beam energy increases quasi-linearly from the head to the tail, which is normal for an underloaded wake, where the acceleration field in the tail is stronger than that experienced by the head of the bunch) with an energy spread of a few percent is generated. Indeed, many schemes based on optimizing the injection and acceleration process in a plasma accelerator have shown this to be the case [18–20]. In the second step, an ideal dechirper is utilized to reduce the energy spread down to 0.1% level without degradation of the beam emittance. In this paper, we propose to use a low-density hollow channel plasma to serve as such a dechirper, as shown in the schematic diagram in Fig. 1.

To see why a hollow channel plasma can act as a near-ideal dechirper, the interaction between the chirped beam and the hollow channel plasma needs to be understood. If the plasma wake wavelength induced by the beam itself in the hollow channel plasma is much longer than its bunch length, the beam will totally stay in a decelerating phase of the wake with a negative slope (the tail of the beam experiences greater energy loss gradient than the head) inside the channel (Fig. 1). For a beam that has an initial positive energy chirp, such a decelerating wake can effectively reduce the positive chirp as the beam propagates through the hollow channel. If the parameters are

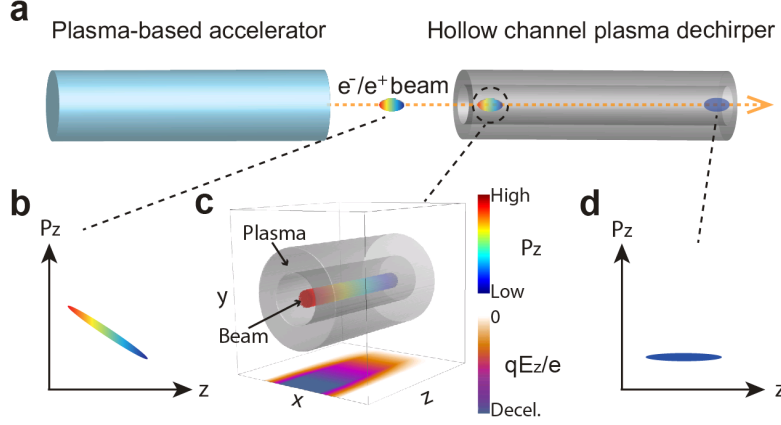


FIG. 1: **Schematic diagram for a near-ideal hollow channel plasma dechirper.** (a) A positively chirped electron/positron beam is generated in a plasma accelerator at first, and then it is sent through a hollow channel plasma to dechirp itself. (b) The initial beam longitudinal phasespace (z versus p_z). (c) The longitudinal wakefield E_z excited by the beam in the hollow channel plasma. The projection in the $x - z$ plane shows the slice of qE_z/e at the mid-plane in the y direction, where q is the particle charge ($-e$ for electron and $+e$ for positron). (d) The final beam longitudinal phasespace (z versus p_z).

properly designed, an energy spread reduction down to 0.1% level or even lower is indeed possible. At the same time, the transverse focusing fields inside the channel will be zero or negligibly small if the beam is launched on or very close to the axis, and this will help to preserve the beam emittance [22]. We also note that this scheme works equally well for electron and positron beams, a unique feature crucial for the application to electron/positron colliders.

In the following sections, detailed theoretical analyses and three-dimensional (3D) particle-in-cell (PIC) simulations will be systematically presented to show the effectiveness of the above scheme on energy spread reduction down to 0.1% level and emittance preservation.

RESULTS

Hollow channel plasma dechirper - concept and PIC simulation illustration. To illustrate the effectiveness of the hollow channel plasma dechirper, we show here one example through 3D PIC simulations using the code QuickPIC [23–25]. In this example, a 10 GeV electron/positron beam with a 1% (RMS) linear positive energy chirp and an intrinsic slice energy spread of 1 MeV (RMS) is sent on-axis through a ~ 78 cm long hollow channel plasma. The beam

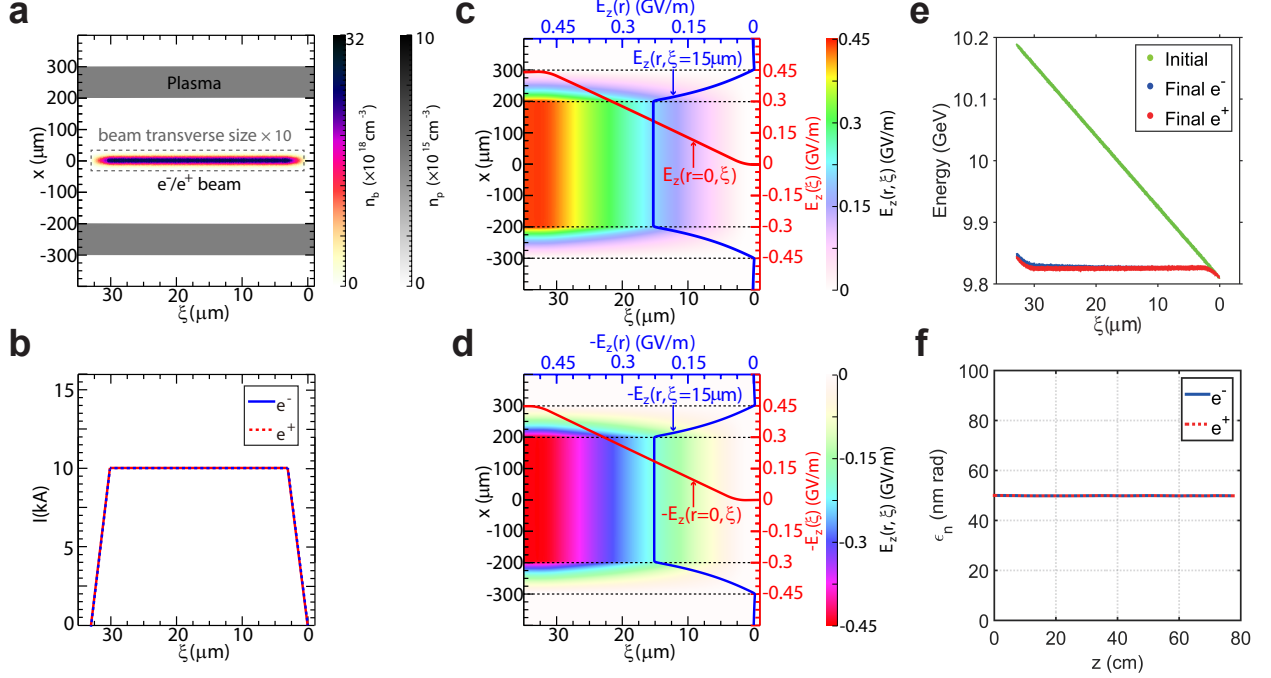


FIG. 2: **3D PIC simulations of the dechirping process with QuickPIC.** (a) The densities of the plasma channel (n_p) and the e⁻/e⁺ beams (n_b) in the $x - \xi$ plane when the propagation distance $z = 1$ cm, where $\xi = ct - z$ represents the longitudinal position relative to the beam. (b) The e⁻/e⁺ beam current profiles (90 fs long plateau, with a 10 fs long ramp at each sides). (c) and (d) show the E_z field excited by the e⁻ and e⁺ bunches, respectively. The black dotted lines represent the inner and outer radii of the plasma channel. Lineouts of the on-axis E_z ($r = 0 \mu\text{m}, \xi$) and the radial variation in E_z ($r, \xi = 15 \mu\text{m}$) are separately shown with red and blue lines. (e) The longitudinal phase spaces of e⁻/e⁺ beams before and after the dechirper. (f) The evolutions of e⁻/e⁺ beam normalized emittances during the dechirping process.

has 1 nC charge with a peak current $I_b = 10$ kA (near flat-top current profile) and low normalized emittance $\epsilon_{nx,y} = 50$ nm rad. As we will see later energy chirps for other current profiles can also be removed but not as completely as for a flat-top pulse. These parameters are chosen to be comparable to the required beam parameters in a future linear collider design [26, 27]. The hollow channel plasma has an inner radius $a = 200 \mu\text{m}$, outer radius $b = 300 \mu\text{m}$, and electron density $n_p = 5 \times 10^{15} \text{ cm}^{-3}$ within the annular plasma ring. By the end of the simulations, the relative energy spreads (δ_W) of both the electron and the positron beams have been dramatically reduced from 1% to $\sim 0.02\%$, close to the intrinsic slice energy spread (0.01%). At the same time, the emittances of the beams remain almost unchanged. Therefore the 6D-brightness of the beam ($B_{6D} = 2I_b/(\epsilon_{nx}\epsilon_{ny}\delta_W) \approx 4.0 \times 10^{19} \text{ Am}^{-2}\text{rad}^{-2}/0.1\%$) has been effectively enhanced by a factor of 50.

The details of the simulations are presented in Fig. 2. The initial densities of the plasma channel and the e^-/e^+ beams are plotted in Fig. 2 (a). The beams have a transverse Gaussian profile with $\sigma_{x,y} = 1.0 \mu\text{m}$, and a near flat-top longitudinal current profile (Fig. 2 (b)). The longitudinal wakefield E_z in the hollow channel plasma excited by the e^-/e^+ beams are shown in Fig. 2 (c) and (d), respectively. One can see that these two fields are very similar except for a change of charge sign, and the on-axis lineouts of both E_z have a near linear deceleration along most of the beam length. The transverse uniformity of E_z within the channel can also be readily seen in Fig. 2 (c) and (d). Combining the above two features of E_z , both beams (e^-/e^+) can be dechirped by the annular plasma with negligible slice energy spread increase. After a propagation of 78.3 cm (e^-)/77.5 cm (e^+), the minimum RMS energy spread of 2.0 MeV (e^-) / 1.7 MeV (e^+) is achieved with a mean energy of 9.83 GeV. Thus the relative energy spreads of the beams have been reduced from 1% down to 0.020% (e^-) / 0.017% (e^+). We note that the subtle differences between the e^- and e^+ beams come from the slightly different nonlinear plasma response [28]. Figure 2 (e) shows the corresponding longitudinal phase spaces of e^- and e^+ bunches before and after the dechirper. Clearly the incoming linear energy chirp has been removed except at the very front and rear of the bunch. In Fig. 2 (f), the evolutions of e^-/e^+ beam normalized emittances over the whole propagation are plotted, and it is evident that the emittances are well conserved. Next we will analyze this concept in details with theoretical analyses and 3D PIC simulations for various beam parameters.

Theory and PIC simulation verification. To quantify the effectiveness of the hollow channel plasma dechirper for various beam parameters, we have carried out a theoretical analysis based on the linear wakefield theory [15, 29]. In the short bunch limit where the wake wavelength is much larger than the beam bunch length, the plasma response to a narrow drive bunch in the hollow channel is relatively weak, therefore the linear plasma wakefield theory can be adopted to properly describe the wakefield structure within the beam.

Using the linear wakefield theory, the longitudinal wakefield E_z in the hollow channel can be expressed as a convolution of the bunch charge distribution with a single-particle wakefunction [14, 28, 29]

$$E_z(r, \xi) = -\frac{q}{e} \frac{mk_p^2 c^2}{e} A_0 \int_{-\infty}^{\xi} d\xi' \cos[\Omega_0 k_p (\xi - \xi')] \frac{I(\xi')}{I_A} \quad (1)$$

where m is the electron rest mass, $k_p = \sqrt{n_p e^2 / m \varepsilon_0 c^2}$ is the plasma wavenumber, ε_0 is the vacuum permittivity, $I(\xi)$ is the the beam current and $I_A \approx 17$ kA is the Alfven current. In this equation, A_0 and Ω_0 are two quantities related to the wake amplitude and wavelength

$$A_0 = \frac{-4B_{00}(a, b)}{k_p a [2B_{10}(a, b) - k_p a B_{00}(a, b)]} \quad (2)$$

$$\Omega_0 = \sqrt{\frac{2B_{10}(a, b)}{2B_{10}(a, b) - k_p a B_{00}(a, b)}} \quad (3)$$

where $B_{ij}(a, b) = I_i(k_p a) K_j(k_p b) + (-1)^{i-j+1} I_j(k_p b) K_i(k_p a)$, and K_n and I_n are the modified Bessel functions of order n .

In the short bunch limit ($k_p L_b \ll 1$), where L_b is the full bunch length, $\cos[\Omega_0 k_p (\xi - \xi')]$ reduces to 1, therefore within the beam, Eq. (1) can be simplified as

$$E_z(r, \xi) \approx -\frac{q}{e} \frac{m k_p^2 c^2}{e} A_0 \frac{I_b}{I_A} \int_0^\xi d\xi' f(\xi') \quad (4)$$

Here $f(\xi)$ is the normalized current profile. Equation (4) shows that E_z is a decelerating field with a negative slope for both e^- and e^+ beams. To quantify the dependence of E_z on the current profile, the expressions of E_z for three typical profiles (flat-top, \sin^2 and Gaussian) are calculated and listed in Table I (see Methods). For the flat-top current profile, E_z within the beam is exactly linear along ξ , which is ideal for completely removing a linear energy chirp. For non-flat-top profiles, nonlinear energy chirps will be induced, therefore the final achievable minimum energy spread ΔW_f will be a trade-off between the linear chirp reduction and the nonlinear chirp growth.

TABLE I: Dechirping effects for three typical current profiles[‡].

	Flat-top	\sin^2	Gaussian
$f(\xi)$	1	$\sin^2(\pi\xi/L_b)$	$e^{-\frac{(\xi-L_b/2)^2}{2 \times (L_b/6)^2} \star}$
$E_z(r, \xi)$	$-\frac{q}{e} \frac{m k_p^2 c^2}{e} A_0 \frac{I_b}{I_A} \xi$	$-\frac{q}{e} \frac{m k_p^2 c^2}{e} A_0 \frac{I_b}{I_A} \times \left[\frac{\xi}{2} - \frac{L_b \sin(2\pi\xi/L_b)}{4\pi} \right]$	$-\frac{q}{e} \frac{m k_p^2 c^2}{e} A_0 \frac{I_b}{I_A} \times \sqrt{\frac{\pi}{72}} L_b \left[1 + \text{Erf} \left(\frac{\xi-L_b/2}{\sqrt{2}L_b/6} \right) \right]^\dagger$
G	$G_F = 0$	$G_S \approx 0.139$	$G_G \approx 0.223$
H	$H_F \approx 3.464$	$H_S \approx 3.430$	$H_G \approx 3.377$

[‡] The subscripts “F”, “S” and “G” refer to the flat-top, \sin^2 and Gaussian current profiles, respectively.

^{*} The RMS bunch length is assumed to be $L_b/6$.

[†] $\text{Erf}(\xi) = \frac{2}{\sqrt{\pi}} \sum_{n=0}^{\infty} \frac{(-1)^n \xi^{2n+1}}{n!(2n+1)}$ is the Gauss error function.

ΔW_f and the required channel length L_c can be calculated as $\Delta W_f = \Delta W_i G$ and $L_c = \frac{\Delta W_i}{|q E_z(r, \xi=L_b)|} H$, where ΔW_i is the initial energy spread (RMS), $E_z(r, \xi = L_b)$ is the longitudinal

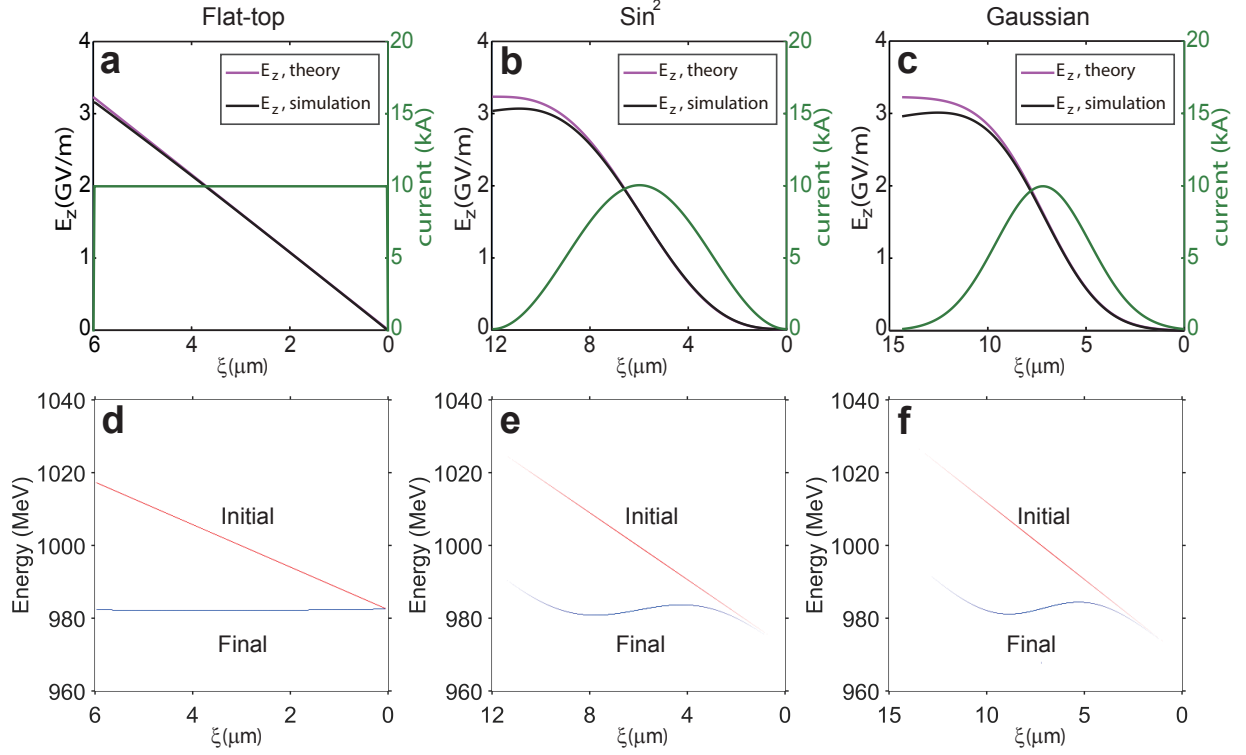


FIG. 3: **Dechirping effects for three typical beam current profiles.** Lineouts of the calculated (in purple) and simulated (in black) E_z field for flat-top (a), \sin^2 (b) and Gaussian (c) current profiles. The corresponding beam longitudinal phasespaces before (in red) and after (in blue) the dechirper for flat-top (d), \sin^2 (e) and Gaussian (f) current profiles. The beam parameters of bunch charge ($Q = 200$ pC), beam peak current ($I_b = 10$ kA), transverse beam size ($\sigma_{x,y} = 1$ μm) and normalized emittance ($\epsilon_{n,x,y} = 50$ nm rad) are all the same for these three cases, which give the corresponding full bunch length L_b ($L_{b,F} = 6$ μm for flat-top, $L_{b,S} = 12$ μm for \sin^2 and $L_{b,G} \approx 14.4$ μm for Gaussian).

electric field at the tail of the beam, G and H are two geometrical factors determined by the beam current profile $f(\xi)$. The expressions of G and H for these three profiles are also listed in Table I (see Methods).

To verify the above theoretical expressions, a series of 3D PIC simulations using the code QuickPIC have been performed. In these simulations, electron beams with different peak currents and profiles are initialized with zero slice energy spread and positive linear energy chirp (mean energy of 1 GeV and relative energy spread of 1% (RMS)). The density of the annular plasma channel is $n_p = 1 \times 10^{17} \text{ cm}^{-3}$ with inner radius $a = 30$ μm and outer radius $b = 60$ μm .

The comparisons of the simulation results with the theoretical expressions are shown in Figs. 3 and 4. Figure 3 (a), (b) and (c) show the very good agreement between the calculated and simulated E_z field for three beam profiles (flat-top, \sin^2 and Gaussian) for a peak current of 10

kA. For lower beam currents, the agreement will be better due to reduced nonlinear effect. The corresponding longitudinal phase spaces before and after the dechirper are shown in Fig. 3 (d), (e) and (f). For the flat-top profile, the longitudinal phase space can be completely flattened, leading to a reduction in relative energy spread from 1% to below 0.01%. For the \sin^2 and Gaussian profiles, E_z still has a linear form for most part of the beam except near the bunch head and tail, where nonlinear feature of the wakefield is evident. This nonlinearity results in a sigmoid structure in the longitudinal phase space of the beam. Despite this non-ideal feature, the relative energy spread can still be reduced significantly from 1% to 0.14% (\sin^2)/0.22% (Gaussian).

The energy spread reduction versus propagation distances are also plotted for these three different profiles in Fig. 4 (a), (b) and (c). It can be clearly seen that the RMS energy spread almost linearly decreases during the beam propagation until the final minimum value is reached. For different peak currents, the achievable minimum RMS energy spreads are almost the same for a given profile, in good accordance with the linear wakefield theory analyses. In Fig. 4 (d) and (e),

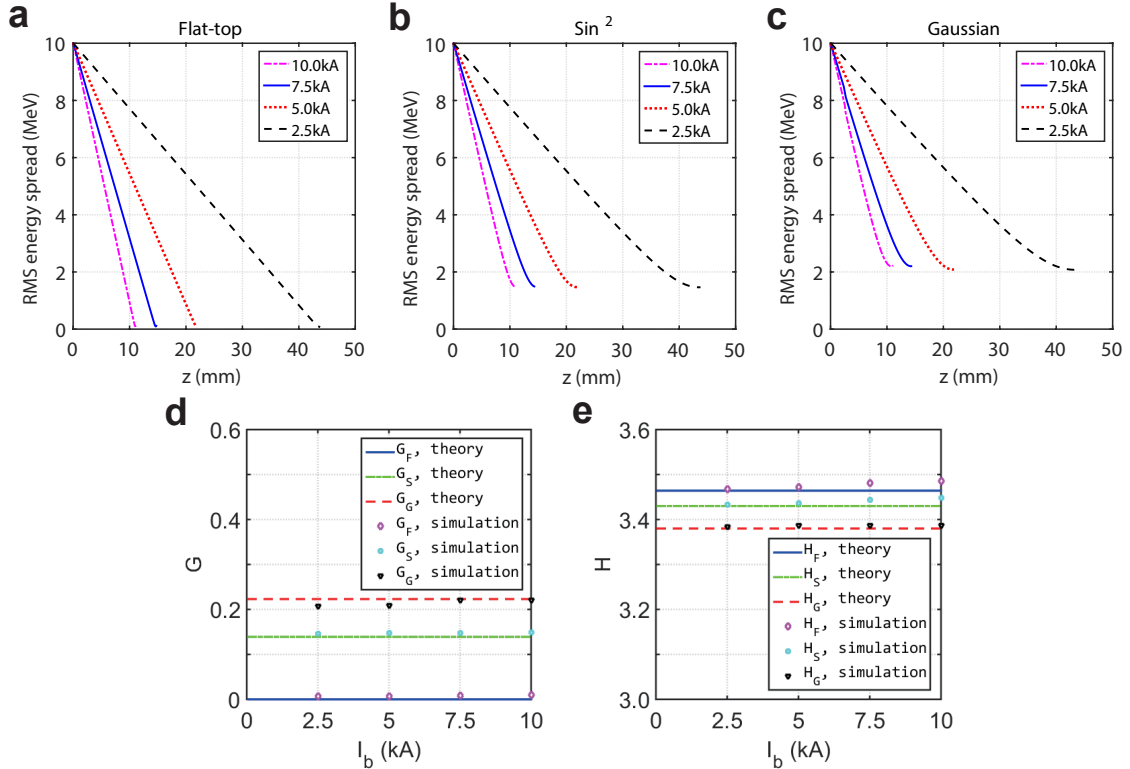


FIG. 4: The RMS energy spread reduction versus the propagation distances for flat-top (a), \sin^2 (b) and Gaussian (c) beam profiles with different peak currents. The other parameters are identical to Fig. 3. The corresponding calculated and simulated geometrical factors G (d) and H (e) are given for these three current profiles.

we also plot the calculated and simulated G and H factors, and an excellent agreement is achieved.

As one can see from above, a flat-top profile for the beam current has the best effect for linear energy chirp reduction, with a potential to obtain energy spread well below 0.1%. Indeed, there are several possibilities in plasma-based acceleration for shaping the beam current profile through injection optimizations [19, 21, 30], and this is a very active research area.

DISCUSSION

The previous sections clearly demonstrate the effectiveness of a hollow channel plasma as a very effective dechirper. In practice, the robustness of this method should also be analyzed. A major factor that will derate the performance of this device, is off-axis injection[31], which will excite a transverse bending field that will steer the beam towards one side. As a result of this deflection, the projected emittance of the beam in the direction of the offset will increase. To quantify the tolerance to off-axis injection, the transverse bending field $W_{\perp} = E_r - cB_{\theta}$ can be calculated for given beam offset and current distribution [28, 31], and it turns out that W_{\perp} is proportional to the offset x_0 and the inner radius a to its -3 power, a^{-3} . The W_{\perp} also has a longitudinal dependence of the beam position, thus in the beam transverse phase space, slice phase-ellipses develop a displacement with respect to each other which increases the projected area and hence leads to the projected emittance growth. In Fig. 5 (a), the final longitudinal phase spaces are plotted for different initial relative beam offset ($x_{0,i}/\sigma_{x,i}$) using 3D PIC simulations with beam and plasma parameters identical to Fig. 2 (a). As expected, small relative offset has a negligible effect on the dechirping process. In Fig. 5 (b), the relative transverse beam offset growth and the relative beam projected emittance growth (in the direction of the offset) versus the initial relative beam offset are plotted. As one can see, the beam offset growth is negligibly small compared to the channel inner radius a , and the beam emittance growth can be controlled to less than $\sim 5\%$ for initial relative beam offset within $\sim 10\%$. In addition to off-axis injection, head-to-tail tilt on an on-axis beam will also lead to transverse wakefields which can induce slice dependent emittance growth. In Fig. 5 (c), the relative beam projected emittance growth (in the direction of the tilt) versus the initial angle of the linear tilt $\theta_{x,i}$ is shown via 3D PIC simulations with the same parameters used in Fig. 2 (a). The beam emittance growth can be controlled to less than $\sim 5\%$ for $\theta_{x,i}$ within ~ 10 mrad. These simulation results suggest that the hollow channel plasma dechirper concept has a reasonably good tolerance for both non-ideal off-axis injection and head-to-tail tilt.

In summary, a new method that uses a hollow channel plasma as a near-ideal dechirper to

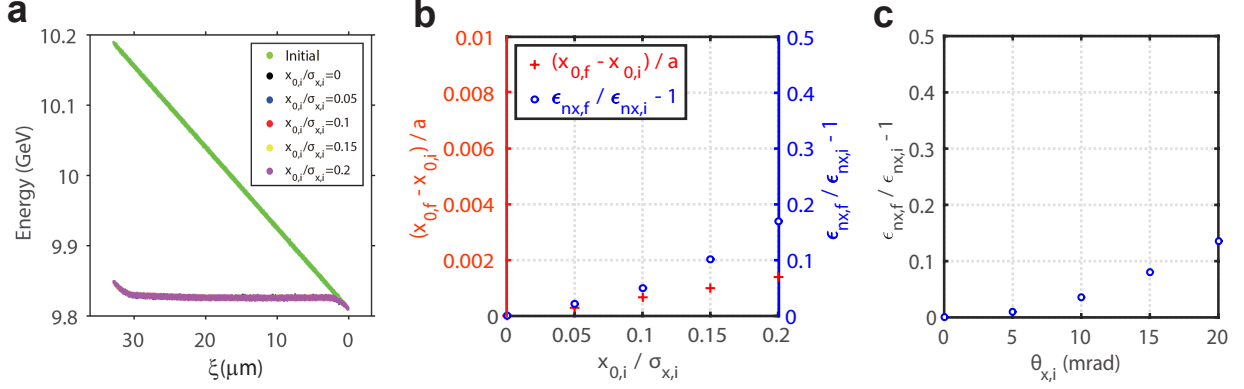


FIG. 5: (a) The simulated initial and final longitudinal phase spaces of the beam for different initial relative beam offset $x_{0,i}/\sigma_{x,i}$. Irrespective of the initial offset, the final longitudinal phase spaces are nearly the same. (b) The relative transverse offset growth of the beam centroid $(x_{0,f} - x_{0,i})/a$ and the projected normalized emittance growth $\epsilon_{nx,f}/\epsilon_{nx,i} - 1$ versus the initial relative beam offset $x_{0,i}/\sigma_{x,i}$, where the subscripts “i” and “f” referring to the initial and final quantities, respectively. (c) The projected normalized emittance growth $\epsilon_{nx,f}/\epsilon_{nx,i} - 1$ versus the initial angle of the linear tilt $\theta_{x,i}$. Note that here we assume the beam offset and the tilt are both in x direction.

reduce the energy chirp of electron and positron beams in plasma-based accelerators is proposed. Theoretical analyses and 3D PIC simulations are systematically used to confirm the effectiveness and robustness of this method for reducing the beam energy spread from a few percent level to ~ 0.1 percent level or lower, while maintaining the beam’s slice energy spread and normalized emittance. This tunable and flexible technique works well for both electron and positron beams, and it can be applied to future plasma-based photon sources and colliders for significantly enhancing the beam 6D-brightnesses.

METHODS

Calculation of the geometrical factors G and H .

To quantify thedechirping effectiveness, the evolution of the beam energy spread has been derived for three typical current profiles (flat-top, \sin^2 and Gaussian). For an electron/positron beam with a linear positive energy chirp and zero intrinsic slice energy spread, its initial energy profile can be expressed as $W(\xi, z = 0) = W_{head,i} + \frac{W_{tail,i} - W_{head,i}}{L_b}\xi$, where $W_{head,i}/W_{tail,i}$ is the initial energy of the beam head/tail. During the dechirping process, since the decelerating field E_z

within the beam has no dependence on r (according to Eq. (4)), the beam energy distribution at the longitudinal positron z can be written as $W(\xi, z) = W(\xi, z = 0) + qE_z(\xi)z$. Thus the mean energy and the RMS energy spread of the beam yield

$$W_{mean}(z) = \frac{\int_0^{L_b} W(\xi, z) f(\xi) d\xi}{\int_0^{L_b} f(\xi) d\xi} \quad (5)$$

and

$$\Delta W(z) = \sqrt{\frac{\int_0^{L_b} [W(\xi, z) - W_{mean}(z)]^2 f(\xi) d\xi}{\int_0^{L_b} f(\xi) d\xi}} \quad (6)$$

When $z = 0$, Eq. (6) gives the initial RMS energy spread ΔW_i . The final minimum RMS energy spread ΔW_f can be achieved when $\frac{d\Delta W(z)}{dz} = 0$ and the corresponding value of z is the required plasma dechirper length L_c .

For the flat-top current profile, i.e., $f(\xi) = 1$ for $0 \leq \xi \leq L_b$. In accordance with Eq. (4), E_z within the beam is exactly linear along ξ

$$E_z(\xi) = -\frac{q}{e} \frac{mk_p^2 c^2}{e} A_0 \frac{I_b}{I_A} \xi \quad (7)$$

Therefore the linear energy chirp of the beam can be completely removed without inducing non-linear energy chirp or slice energy spread, yielding zero ΔW_f , i.e., $G_F = 0$. The plasma dechirper length $L_{c,F}$ can be intuitively obtained as $L_{c,F} = \frac{W_{tail,i} - W_{head,i}}{|qE_z(\xi=L_b)|}$. Indeed, to make a comparison between different current profiles, we should keep ΔW_i fixed. In this case, according to Eq. (6), $W_{tail,i} - W_{head,i} \approx 3.464\Delta W_i$, therefore $L_{c,F}$ can be rewritten in terms of ΔW_i as

$$L_{c,F} = \frac{\Delta W_i}{|qE_z(\xi=L_b)|} H_F = \frac{\Delta W_i}{mk_p^2 c^2 A_0 \frac{I_b}{I_A} L_b} H_F \quad (8)$$

where $H_F \approx 3.464$.

For the \sin^2 current profile, i.e., $f(\xi) = \sin^2(\pi\xi/L_b)$. According to Eq. (4), the expression for E_z is

$$E_z(\xi) = -\frac{q}{e} \frac{mk_p^2 c^2}{e} A_0 \frac{I_b}{I_A} \times \left[\frac{\xi}{2} - \frac{L_b \sin(2\pi\xi/L_b)}{4\pi} \right] \quad (9)$$

One can see the first term in the brackets is the linear term of ξ , while the second term is the high-order nonlinear correction, which leads to the nonlinear energy chirp growth. After obtaining the expression for $\Delta W(z)$ and setting $\frac{d\Delta W(z)}{dz} = 0$, we find $G_S \approx 0.139$ and $L_{c,S} \approx \frac{W_{tail,i} - W_{head,i}}{|qE_z(\xi=L_b)|} \times 0.6201$. Based on Eq. (6), $W_{tail,i} - W_{head,i} \approx 5.532\Delta W_i$, thus $L_{c,s}$ yields

$$L_{c,S} = \frac{\Delta W_i}{|qE_z(\xi=L_b)|} H_S = \frac{\Delta W_i}{mk_p^2 c^2 A_0 \frac{I_b}{I_A} \frac{L_b}{2}} H_S \quad (10)$$

where $H_S \approx 0.6201 \times 5.532 \approx 3.430$.

For the Gaussian current profile, the beam is assumed to be cut off outside three standard deviations from the beam center, i.e., $f(\xi) = e^{-\frac{(\xi-L_b/2)^2}{2 \times (L_b/6)^2}}$. Substituting $f(\xi)$ into Eq. (4), E_z within the beam can be expressed as

$$E_z(\xi) = -\frac{q}{e} \frac{mk_p^2 c^2}{e} A_0 \frac{I_b}{I_A} \times \sqrt{\frac{\pi}{72}} L_b \left[1 + \text{Erf} \left(\frac{\xi - L_b/2}{\sqrt{2} L_b/6} \right) \right] \quad (11)$$

Since the Gauss error function has both the linear and nonlinear terms, high-order nonlinear energy chirp will increase during the dechirping process. Similar to the \sin^2 current profile case, we can obtain $G_G \approx 0.223$ and $L_{c,G} \approx \frac{W_{tail,i} - W_{head,i}}{|qE_z(\xi=L_b)|} \times 0.5553$. From Eq. (6) we have $W_{tail,i} - W_{head,i} \approx 6.081 \Delta W_i$, hence $L_{c,G}$ is given by

$$L_{c,G} = \frac{\Delta W_i}{|qE_z(L_b)|} H_G = \frac{\Delta W_i}{mk_p^2 c^2 A_0 \frac{I_b}{I_A} \sqrt{2\pi} L_b/6} H_G \quad (12)$$

where $H_G \approx 0.5553 \times 6.081 \approx 3.377$.

3D PIC Simulations.

The simulations are carried out using the 3D quasi-static PIC code QuickPIC [23–25] in Cartesian coordinates with a window moving at the speed of light in the beam direction (z axis).

In the simulations shown in Fig. 2, the simulation box has a size of $36 \mu\text{m} \times 800 \mu\text{m} \times 800 \mu\text{m}$, divided into $512 \times 1024 \times 1024$ cells along the z , y and x direction, respectively. The beam contains 3.4×10^7 macro-particles and the plasma contains 5.4×10^8 macro-particles. The beam evolution step size is $4k_p^{-1}$.

In the simulations shown in Figs. 3 and 4, the simulation box consists of $512 \times 512 \times 512$ cells. The number of beam macro-particles is 1.7×10^7 and the number of plasma macro-particles is 1.3×10^8 . The beam evolution step size is $2k_p^{-1}$. For the flat-top current profile, the size of the simulation box is $6 \mu\text{m}$ (in z) \times $200 \mu\text{m}$ (in y) \times $200 \mu\text{m}$ (in x). For the \sin^2 current profile, the size of the simulation box is $12 \mu\text{m}$ (in z) \times $200 \mu\text{m}$ (in y) \times $200 \mu\text{m}$ (in x). For the Gaussian current profile, the size of the simulation box is $15 \mu\text{m}$ (in z) \times $200 \mu\text{m}$ (in y) \times $200 \mu\text{m}$ (in x).

ACKNOWLEDGMENTS

This work was supported by the NSFC Grants No. 11535006, No. 11425521, No. 11775125, No. 11475101, the U.S. DOE Grants No. DE-SC0010064, No. DE-SC0014260, No. DE-SC0008491,

No. DE- SC0008316 and the U.S. NSF Grants No. 1500630, No. 1734315, No. ACI-1339893, No. ACI-1614949, No. ACI-1713760, No. PHY-1415386, No. PHY-500630. The numerical simulations were carried out using Sunway TaihuLight cluster at National Supercomputing Center in Wuxi (NSCCWX).

REFERENCES

* jfhua@tsinghua.edu.cn

† weilu@tsinghua.edu.cn

- [1] T. Tajima and J. M. Dawson, Phys. Rev. Lett. **43**, 267 (1979).
- [2] P. Chen, J. M. Dawson, R. W. Huff, and T. Katsouleas, Physical Review Letters **54**, 693 (1985), URL <https://link.aps.org/doi/10.1103/PhysRevLett.54.693>.
- [3] S. P. D. Mangles, C. D. Murphy, et al., Nature **431(7008)**, 535 (2004).
- [4] C. G. R. Geddes, C. Toth, et al., Nature **431(7008)**, 538 (2004).
- [5] J. Faure, Y. Glinec, et al., Nature **431(7008)**, 541 (2004).
- [6] W. Leemans et al., Nature Phys. **2**, 696 (2006).
- [7] N. A. M. Hafz, T. M. Jeong, et al., Nature Photonics **2(9)**, 571 (2008).
- [8] X. Wang, R. Zgadzaj, et al., Nature communications **4**, 1988 (2013).
- [9] K. H. P. Hyung Taek Kim et al., Phys. Rev. Lett. **111**, 165002 (2013).
- [10] W. P. Leemans, A. J. Gonsalves, et al., Phys. Rev. Lett **113**, 245002 (2014).
- [11] I. Blumenfeld et al., Nature **445**, 741 (2007).
- [12] M. Litos, E. Adli, et al., Nature **515(7525)**, 92 (2014).
- [13] S. Corde, E. Adli, et al., Nature **524**, 442 (2015).
- [14] S. Gessner, E. Adli, et al., Nature Communications **7**, 11785 (2016).
- [15] T. Katsouleas, S. Wilks, et al., Particle Accelerators **22**, 81 (1987).
- [16] M. Tzoufras et al., Phys. Rev. Lett. **101**, 145002 (2008).
- [17] F. Li, C. J. Zhang, et al., Plasma Phys. Control. Fusion **58**, 034004 (2016).
- [18] X. L. Xu, Y. P. Wu, et al., Phys. Rev. ST Accel. Beams **17**, 061301 (2014).
- [19] F. Li, J. F. Hua, et al., Phys. Rev. Lett. **111**, 015003 (2013).
- [20] Y. Wan, C. J. Zhang, et al., Plasma Phys. Control. Fusion **58**, 034015 (2016).
- [21] X. L. Xu, F. Li, et al., Phys. Rev. ST Accel. Beams **20**, 11303 (2017).
- [22] T. C. Chiou and T. Katsouleas, Physical review letters **81**, 3411 (1998).
- [23] C. Huang et al., J. Phys. Confer. Series **46**, 190 (2006).
- [24] W. An et al., J. Comput. Phys. **250**, 165 (2013).

- [25] *Quickpic open source*, <https://github.com/UCLA-Plasma-Simulation-Group/QuickPIC-OpenSource>.
- [26] *The International Linear Collider Technical Design Report* (2013), <http://www.linearcollider.org/ILC/Publications/Technical-Design-Report>.
- [27] C. B. Schroeder, E. Esarey, et al., Physical Review Special Topics-Accelerators and Beams **13**, 101301 (2010).
- [28] S. Gessner, Ph.D. thesis, Stanford University (2016).
- [29] C. B. Schroeder, D. H. Whittum, et al., Phys. Rev. Lett. **82**, 1177 (1999).
- [30] X. L. Xu et al., Phys. Rev. Lett. **112**, 035003 (2014).
- [31] C. A. Lindström, E. Adli, et al., Physical review letters **120**, 124802 (2018).